Fractal frequency spectrum in laser resonators and three-dimensional geometric topology of optical coherent waves

J. C. Tung,[1] P. H. Tuan,[1] H. C. Liang,[2] K. F. Huang,[1] and Y. F. Chen[1,*]

[1]*Department of Electrophysics, National Chiao Tung University, 1001 Ta-Hsueh Road, Hsinchu 30010, Taiwan*

[2]*Institute of Optoelectronic Science, National Taiwan Ocean University, 2 Pei-Ning Road, Keelung 20224, Taiwan*

(Received 10 May 2016; published 3 August 2016)

We theoretically verify that the symmetry breaking in spherical resonators can result in a fractal frequency spectrum that is full of numerous new accidental degeneracies to cluster around the unperturbed degenerate cavity. We further experimentally discover that the fractal frequency spectrum excellently reflects the intimate connection between the emission power and the degenerate mode numbers. It is observed that the wave distributions of lasing modes at the accidental degeneracies are strongly concentrated on three-dimensional (3D) geometric topology. Considering the overlapping effect, the wave representation of the coherent states is analytically derived to manifest the observed 3D geometric surfaces.

DOI: 10.1103/PhysRevA.94.023811

I. INTRODUCTION

Starting from Mandelbrot's seminal discovery [1], self-similar and fractal structures have been observed in a variety of phenomena in nature [2] and have also been found in many branches of physics [3–5]. One of the prominent examples in quantum systems is the fractal conductance fluctuations in gold nanowires and in mesoscopic electron billiards [6–10]. Another prominent example of the self-similar phenomena is the plateau formation in the transverse Hall-resistance curve of a two-dimensional (2D) electron system at low temperatures in the presence of a strong perpendicular magnetic field, known as the quantum Hall effect [11,12]. More intriguingly, the Hofstadter's fractal energy spectrum [13,14] for Landau levels in a 2D periodic lattice has been realized [15,16].

The remarkable analogy between optical and mechanical phenomena was fully developed in Hamilton's ingenious opticomechanical theory that played a fundamental role in the development of ideas in quantum physics [17–20]. Thanks to the development of modern laser cavities, not only eigenvalues but also eigenfunctions have been analogously explored by using solid-state lasers for a 2D quantum harmonic oscillator [21–25] and semiconductor lasers for 2D quantum billiards [26–30]. Optical resonators with the same isomorphism clearly confirm that the level degeneracies in 2D mesoscopic quantum systems generally lead to the wave functions with intensities concentrated on classical periodic orbits [10]. Nevertheless, optical resonators have never been used to explore the energy spectrum in higher-dimensional quantum systems. In particular, the emergence of the ray geometry from the coherent wave in optical resonators is still an open and fascinating issue of active research in recent years. The attractive interest comes partly from the fundamental questions of light-matter interaction [31] and ray-wave correspondence [32–34], and partly from numerous applications, such as cavity spectroscopy [35–37], optical pattern formation [38–41], single-photon emitters [42], and ultralow threshold lasers [43,44].

One of the earlier reports on laser fractals was to demonstrate that the eigenmodes of unstable-cavity lasers have fractal structure [45]. The spatial fractal formation for laser transverse modes was later confirmed in so-called kaleidoscope lasers that include nontrivial transverse boundary conditions [46,47]. In contrast with the eigenmode fractal formation in the unstable cavity, we here explore the eigenfrequency fractal formation in the stable spherical cavity subject to the parasitic astigmatism. In this work we theoretically verify that the symmetry breaking induced by astigmatism leads to a fractal frequency spectrum in laser resonators. The fractal frequency spectrum is found to display numerous new accidental degeneracies at the cavity lengths near the unperturbed degenerate cavity. We further exploit the selective pumping to excite the astigmatic resonator and experimentally discover that the emission power variation on the cavity length exhibits the local maxima at the accidental degeneracies to form a fractal fluctuation corresponding to the fractal frequency spectrum. It is also observed that the wave distributions of lasing modes at the accidental degeneracies are remarkably concentrated on the three-dimensional (3D) geometric surfaces. Finally, we theoretically derive the coherent states to manifest the 3D geometric topology of the lasing modes. Based on the opticomechanical analogy, the present results can be directly applied to the 3D integrable quantum systems with symmetry breaking to explore the wave functions related to 3D geometric surfaces.

II. FRACTAL FREQUENCY SPECTRUM

In a laser resonator with the gain medium, the inevitable symmetry breaking comes from the astigmatism induced by the birefringence of the gain medium and the angle of the beam divergence. As a consequence, the eigenfrequencies of the spherical cavity with parasitic astigmatism can be generally given by

$$\omega_{m,n,\ell} = \ell\omega_z + (m+1/2)\omega_{t,x} + (n+1/2)\omega_{t,y}, \qquad (1)$$

where ℓ is the longitudinal mode index, m and n are the transverse mode indices, ω_z is the longitudinal mode spacing, and $\omega_{t,x}$ and $\omega_{t,y}$ are the transverse mode spacings in the x and

*Department of Electrophysics, National Chiao Tung University, 1001 Ta-Hsueh Road, Hsinchu 30010, Taiwan; yfchen@cc.nctu.edu.tw.

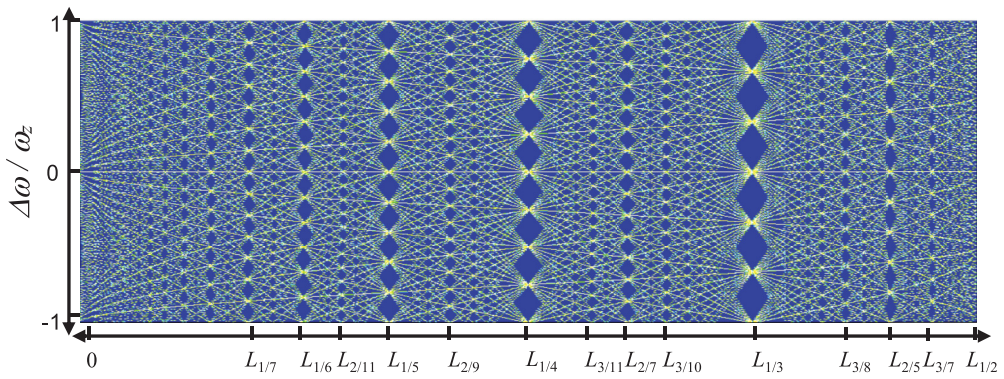

FIG. 1. Frequency spectrum $\omega_{m,n,\ell}$ of the ideal spherical cavity in the neighborhood of the indices (m_o,n_o,ℓ_o) as a function of the normalized cavity length L_t/R for the range of $|m-m_o| \leqslant 12$, $|n-n_o| \leqslant 12$, and $|\ell-\ell_o| \leqslant 12$.

y directions. For the concave-plano resonator, the transverse mode spacings are given by $\omega_{t,x} = (\omega_z/\pi)\sin^{-1}\sqrt{L_{t,x}/R}$ and $\omega_{t,y} = (\omega_z/\pi)\sin^{-1}\sqrt{L_{t,y}/R}$, where $\omega_z = c/2L_{\rm opt}$, $L_{\rm opt} = L_{\rm cav} + (n_r - 1)L_g$, n_r is the refractive index of the gain medium, L_g is the physical length of the gain medium, and R is the curvature radius of the concave mirror. Due to the symmetry breaking, the effective cavity lengths can be generally expressed as $L_{t,x} = L_t - d/2$ and $L_{t,y} = L_t + d/2$, where L_t is the mean value of $L_{t,x}$ and $L_{t,y}$ and d I s the difference between $L_{t,x}$ and $L_{t,y}$.

Neglecting the astigmatic effect, L_t is given by $L_t = L_{\rm cav} + [n_r - (1/n_r)]L_g$ and $d = 0$. Under this circumstance, $\omega_{t,x} = \omega_{t,y} = \omega_t = (\omega_z/\pi)\sin^{-1}\sqrt{L_t/R}$ and the frequency spectrum $\omega_{m,n,\ell}$ in the neighborhood of the indices (m_o,n_o,ℓ_o) is given by

$$\left(\frac{\Delta\omega}{\omega_z}\right) = [(m+n) - (m_o+n_o)]\left(\frac{\omega_t}{\omega_z}\right) + (\ell - \ell_o), \quad (2)$$

where $\Delta\omega = \omega_{m,n,\ell} - \omega_{m_o,n_o,\ell_o}$ is the frequency difference. The frequency ratio ω_t/ω_z is a monotonically increasing function of the effective cavity length L_t for a given R and its value is between 0 and 1/2 for $0 \leqslant L_t \leqslant R$. Note that the relationship between $\Delta\omega/\omega_z$ and ω_t/ω_z in Eq. (2) is a simple Diophantine equation. The occurrence of degeneracy is given by $\Delta\omega = 0$ in Eq. (2). Figure 1 shows the frequency spectrum $\omega_{m,n,\ell}$ in the neighborhood of the indices (m_o,n_o,ℓ_o) as a function of the effective cavity length L_t for $R = 10$ mm. It can be seen that the degeneracies and gaps appear at the effective cavity length $L_t = L_{P/Q}$ that leads to the frequency ratio of ω_t/ω_z corresponding to the rational number P/Q, where P and Q are coprime integers. The family of the degenerate states can be in terms of the triple integers (p,q,s) to express the mode indices (m,n,ℓ) as $m = m_o + pu$, $n = n_o + qu$, and $\ell = \ell_o + su$, where the integer u is a common index given by $u = \cdots -2, -1, 0, 1, 2\cdots$. Using Eq. (2), the triple integers (p,q,s) for the degenerate condition of $\omega_t/\omega_z = P/Q$ can be shown to satisfy a simple relation $(p+q)(P/Q) + s = 0$ that indicates that $p + q = MQ$ and $s = -MP$, where M is an integer.

Figure 2(a) shows the influence of the symmetry breaking on the frequency spectrum $\omega_{m,n,\ell}$ for an example of $R = 10$ mm and $d = 50\,\mu$m. It is clear that the parasitic astigmatism gives rise to the level rearrangement and breaks the original degeneracies at $L_t = L_{P/Q}$ in the unperturbed spherical cavity. Nevertheless, there are numerous new degeneracies to appear in the neighborhood of $L_t = L_{P/Q}$, as shown in Fig. 2(b). To reveal the new degeneracies near the region of $L_t = L_{P/Q}$, a dimensionless parameter ξ is introduced to express the effective cavity length as $L_t = L_{P/Q} + \xi\, d$, where $|\xi| \leqslant 1$. Using the parameter ξ and the property $d \ll R$, the transverse frequencies near $L_t = L_{P/Q}$ can be derived as

$$\frac{\omega_{t,x}}{\omega_z} = \frac{P}{Q} + \beta\left(\xi - \frac{1}{2}\right), \quad \frac{\omega_{t,y}}{\omega_z} = \frac{P}{Q} + \beta\left(\xi + \frac{1}{2}\right), \quad (3)$$

where $\beta = d/[\pi R \sin(2\pi P/Q)]$. Substituting Eq. (3) into Eq. (1) and using the triple integers (p,q,s) with the identity of $(p+q)(P/Q) + s = 0$, the frequency spectrum near $L_t = L_{P/Q}$ with respect to ω_{m_o,n_o,ℓ_o} can be simplified as

$$\left(\frac{\Delta\omega}{\omega_z}\right) = \beta u\left[(p+q)\xi - \frac{1}{2}(p-q)\right]. \quad (4)$$

Note that the relationship between $\Delta\omega/\omega_z$ and ξ in Eq. (4) is also a Diophantine equation. The criterion $\Delta\omega = 0$ in Eq. (4) gives the new accidental degeneracies to occur at the effective cavity lengths $L_t = L_{P/Q} + \xi\, d$ with

$$\xi = \frac{1}{2}\frac{(p-q)}{(p+q)}. \quad (5)$$

Numerous integer pairs (p,q) for the new degeneracies are shown in Fig. 2(b). Substituting Eq. (5) into Eq. (3), it can be found that

$$\frac{\omega_{t,x}}{\omega_z} = \frac{P}{Q} - \beta\frac{q}{p+q}, \quad \frac{\omega_{t,y}}{\omega_z} = \frac{P}{Q} + \beta\frac{p}{p+q}. \quad (6)$$

As discussed later, Eq. (6) plays an important role in manifesting the topological geometry of the coherent states.

Now we discuss the fractal dimension of the frequency spectrum shown in Fig. 2. The frequency spectrum is related to the degeneracy distribution of the cavity length. Without the astigmatic effect, $d = 0$, there are no additional degenerate points in the frequency spectrum; consequently, the fractal dimension is zero. When $d \neq 0$, the value of the fractal dimension is between 0 and 1, similar to that of the Cantor set. Using the definition that fractal dimension D equals the log of the number of pieces N divided by the log of the magnification factor r, the fractal dimension of the frequency spectrum can

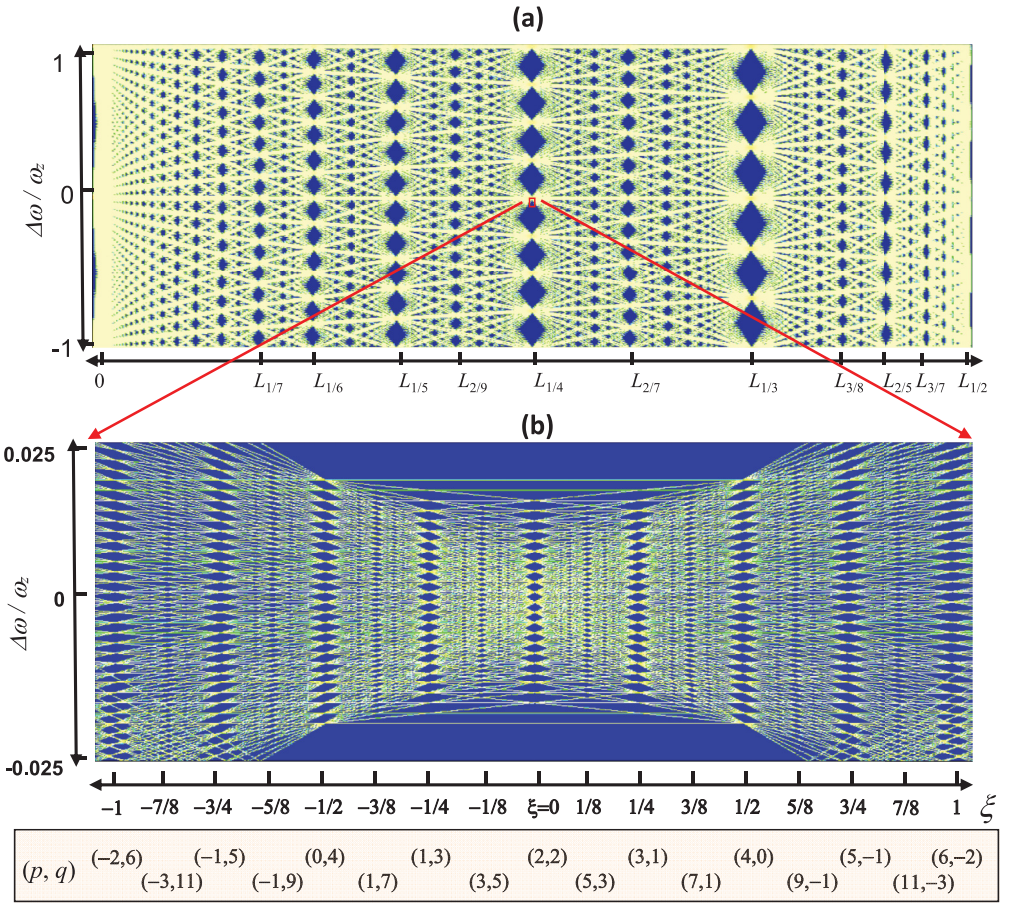

FIG. 2. (a) Influence of the symmetry breaking on the frequency spectrum $\omega_{m,n,\ell}$ for an example of $R = 10\,\text{mm}$ and $d = 50\,\mu\text{m}$ for the range of $|m - m_o| \leqslant 12$, $|n - n_o| \leqslant 12$, and $|\ell - \ell_o| \leqslant 12$. (b) Partial magnification of the frequency spectrum in the neighborhood of $L_t = L_{P/Q}$ with $P/Q = 1/4$.

be expressed as $D = \log(N)/\log(r)$. As shown in Fig. 2, the magnification factor is given by $r = R/d$. From Eq. (6), the number of pieces N can be estimated to be $N = P/(MQ\beta)$, where the multiplication factor M is related to $p + q = MQ$. The maximum multiplication factor is usually not greater than 5. For a typical example of $R = 10\,\text{mm}$ and $d = 50\,\mu\text{m}$, the mean fractal dimension D is calculated to be 0.745 for $M = 1$, 0.594 for $M = 2$, and 0.506 for $M = 3$. It can be seen that the overall characteristics of the fractal dimension are rather close to that of the Cantor set [48].

III. EXPERIMENTAL OBSERVATIONS

To explore the effect of the fractal frequency spectrum, we exploited the off-center selective pumping to excite extremely high-order modes in a solid-state laser, as shown in Fig. 3 for the setup. The cavity was formed by a concave mirror and a gain medium. For the concave mirror, the radius of curvature is $R = 10\,\text{mm}$ and the reflectivity is 99.8% at the wavelength of 1064 nm. The concave mirror was precisely controlled to vary the cavity length in the range of 3.8–8.8 mm. The gain medium was an a-cut 2.0−at.% Nd^{3+}: YVO_4 crystal with a length of 2 mm. One side of the gain medium was coated for antireflection at 808 nm and 1064 nm (reflection <0.1%) and the other side was coated to be an output coupler with a transmission of 0.5% at 1064 nm. The pump source was an 808-nm fiber-coupled laser diode with a core diameter of 100 μm, a numerical aperture of 0.16, and a maximum output power of 3 W. A focusing lens was used to reimage the pump beam into the gain medium with the off-center displacement of $\Delta x = 0.7\,\text{mm}$ and $\Delta y = 0.56\,\text{mm}$. The emission power was systematically recorded by changing the cavity length with a precise step of 10 μm.

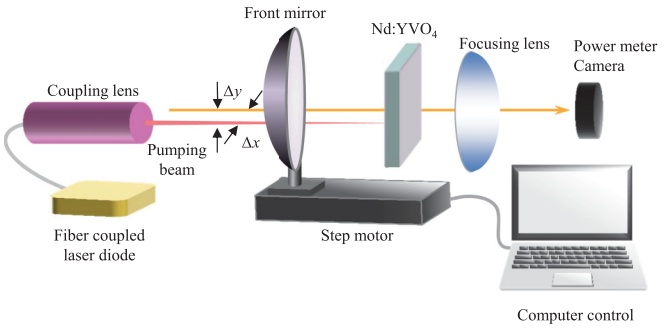

FIG. 3. Experimental laser setup with the off-center selective pumping to excite extremely high-order transverse modes for exploring the effect of the fractal frequency spectrum.

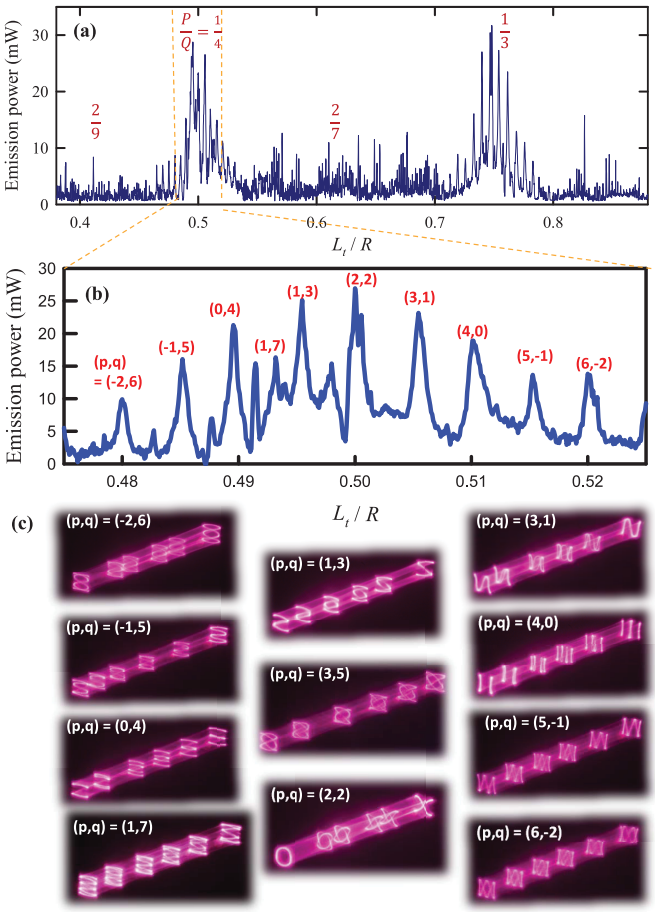

FIG. 4. (a) Experimental result for the emission power as a function of the cavity length under a pump power of 1.0 W. (b) Partial magnification of the power variation in the region of $P/Q = 1/4$. (c) Experimentally tomographic images of the lasing modes at the main peaks of the emission power.

Since the emission power is generally proportional to the number of the excited cavity modes, the emission power has an intimate connection with the degeneracy. Figure 4(a) shows the experimental result for the emission power as a function of the cavity length under a pump power of 1.0 W. It is clear that the emission power variation on the cavity length exhibits the local maxima at the accidental degeneracies to form a fractal fluctuation corresponding to the fractal frequency spectrum. Figure 4(b) shows the partial magnification of the power variation in the region of $P/Q = 1/4$. The experimentally tomographic images of the lasing modes at the main peaks of the emission power are shown in Fig. 4(c). The tomographic images of the lasing modes were obtained by controlling the exposure time of the camera to selectively capture the transverse patterns inside the cavity along the longitudinal propagation. More specifically, a pair of relay lenses was used to reimage the laser modes onto a paper screen that was moved by tracking the camera to record the tomographic images. The transverse patterns can be clearly seen to be localized on the Lissajous curves with specific indices (p,q) related to the degeneracies shown in Fig. 2(b). In the following, it is theoretically shown that the formation of the lasing modes can be nicely represented by using the quantum coherent states.

IV. MANIFESTING 3D GEOMETRIC TOPOLOGY OF LASER MODES

Considering the paraxial approximation and the astigmatism between the x and y directions, the eigenmodes for the laser cavity with a concave mirror at $z = -L_{\rm opt}$ and a plane mirror at $z = 0$ can be divided into two waves traveling in opposite directions: $\Phi_{m,n,\ell} = [\Phi^{(+)}_{m,n,\ell} - \Phi^{(-)}_{m,n,\ell}]/\sqrt{2}$, where

$$\Phi^{(\pm)}_{m,n,\ell}(x,y,z,t) = \mathrm{X}_m(x,z)e^{-i(m+1/2)\theta^{(\pm)}_{t,x}(\tilde{z},t)}\mathrm{Y}_n(y,z) \times e^{-i(n+1/2)\theta^{(\pm)}_{t,y}(\tilde{z},t)}e^{-i\ell\theta^{(\pm)}_{L}(\tilde{z},t)}, \quad (7)$$

with

$$\mathrm{X}_m(x,z) = \sqrt{\sqrt{2/\pi}/[w_x(z)2^m m!]}e^{-\tilde{x}^2/2}H_m(\tilde{x}), \quad (8)$$

$$\mathrm{Y}_n(y,z) = \sqrt{\sqrt{2/\pi}/[w_y(z)2^n n!]}e^{-\tilde{y}^2/2}H_n(\tilde{y}), \quad (9)$$

$$\theta^{(\pm)}_{t,x}(\tilde{z},t) = (\omega_{t,x}/\omega_z)\theta^{(\pm)}_z(\tilde{z},t) \mp \theta_{G,x}(z), \quad (10)$$

$$\theta^{(\pm)}_{t,y}(\tilde{z},t) = (\omega_{t,y}/\omega_z)\theta^{(\pm)}_z(\tilde{z},t) \mp \theta_{G,y}(z). \quad (11)$$

$\theta^{(\pm)}_z(\tilde{z},t) = \omega_z(t \pm \tilde{z}/c)$, $H_m(\cdot)$ are the Hermite polynomials of order m, $\tilde{x} = \sqrt{2}x/w_x(z)$, $\tilde{y} = \sqrt{2}y/w_y(z)$, $w_x(z) = w_{o,x}\sqrt{1+(z/z_{R,x})^2}$, $w_y(z) = w_{o,y}\sqrt{1+(z/z_{R,y})^2}$, $w_{o,x} = \sqrt{2z_{R,x}/k_{m,n,\ell}}$, $w_{o,y} = \sqrt{2z_{R,y}/k_{m,n,\ell}}$, $z_{R,x} = \sqrt{L_{t,x}(R-L_{t,x})}$, $z_{R,y} = \sqrt{L_{t,y}(R-L_{t,y})}$, $\tilde{z} = z\{1+[x^2/2(z^2+z^2_{R,x})]+[y^2/2(z^2+z^2_{R,y})]\}$, $\theta_{G,x}(z) = \tan^{-1}(z/z_{R,x})$, and $\theta_{G,y}(z) = \tan^{-1}(z/z_{R,y})$.

Based on the completeness of the basis states, the general representation for the wave function can be expressed as $\Psi^{(\pm)}(x,y,z,t) = \sum_\ell \sum_n \sum_m c_\ell b_n a_m \Phi^{(\pm)}_{m,n,\ell}(x,y,z,t)$, where a_m and b_n are the amplitude coefficients for the transverse orders m and n and c_ℓ is the amplitude coefficient for the longitudinal order ℓ. It has been shown that the longitudinal modes in an end-pumped standing-wave cavity are primarily related to the spatial hole burning (SHB) effect [49]. The strength of the SHB effect is mainly determined by the separation between the gain medium and the input mirror. The stronger the SHB effect, the more the longitudinal lasing modes. Here it is conveniently assumed that there are $2N+1$ longitudinal modes to be excited and $c_\ell = 1/(2N+1)$ for $|\ell - \ell_o| \leqslant N$ and $c_\ell = 0$ for $|\ell - \ell_o| > N$. It has been shown [34] that the coefficients $a_m b_n$ are mainly controlled by the spatial overlap between the transverse mode $\mathrm{X}_m(x,z)\mathrm{Y}_n(y,z)$ and the distribution of the pump source $F(x,y)$; i.e.,

$$a_m b_n = \iint \mathrm{X}_m(x,z_c)\mathrm{Y}_n(y,z_c)F(x,y)dxdy, \quad (12)$$

where z_c is the location of the gain medium. Considering a selective pumping with the transverse displacements Δx and Δy in the x and y directions, the pump distribution $F(x,y)$ can be modeled as [34]

$$F(x,y) = \sqrt{\frac{2}{\pi}}\sqrt{\frac{1}{w_x(z_c)w_y(z_c)}}e^{-(x-\Delta x)^2/w^2_x(z_c)}e^{-(y-\Delta y)^2/w^2_y(z_c)}. \quad (13)$$

Substituting Eqs. (8), (9), and (13) into Eq. (12) and using the generating function of the Hermite polynomials [50], the coefficients can be derived as $a_m = (m_o)^{m/2}e^{-m_o/2}/\sqrt{m!}$ and $b_n = (n_o)^{n/2}e^{-n_o/2}/\sqrt{n!}$, where $m_o = [\Delta x/w_x(z_c)]^2$ and $n_o = [\Delta y/w_y(z_c)]^2$. Note that the values of the parameters m_o and n_o signify the magnitudes of the off-center displacements in the x and y directions, respectively. The expression for a_m and b_n is exactly the form of the square root of the Poisson distribution. For convenience, we take the parameters m_o and n_o to be the integers closest to the values of $[\Delta x/w_x(z_c)]^2$ and $[\Delta y/w_y(z_c)]^2$, respectively.

Using the property of the Schrödinger coherent state and the expressions for the coefficients a_m, b_n, and c_ℓ, the intensity of the wave-packet state $I^{(\pm)}=|\Psi^{(\pm)}(x,y,z,t)|^2$ can be derived as

$$I^{(\pm)}(x,y,z,t) = \frac{2}{\pi w_x(z)w_y(z)} e^{-\{\tilde{x}-\sqrt{2}\sqrt{m_o}\cos[\theta_{t,x}^{(\pm)}(\tilde{z},t)]\}^2} e^{-\{\tilde{y}-\sqrt{2}\sqrt{n_o}\cos[\theta_{t,y}^{(\pm)}(\tilde{z},t)]\}^2} \left\{\frac{\sin[(2N+1)\theta_z^{(\pm)}(\tilde{z},t)/2]}{\sin[\theta_z^{(\pm)}(\tilde{z},t)/2]}\right\}^2. \tag{14}$$

The analytical form in Eq. (14) can straightforwardly be exploited to establish the ray-wave connection. First of all, since the total number of longitudinal modes is fairly greater than 1, i.e., $N \gg 1$, the term involving the sine function in Eq. (14) leads the intensity of the wave packet to concentrate at $\theta_z^{(\pm)}(\tilde{z},t) = 2\pi u$ for any integers u. Substituting $\theta_z^{(\pm)}(\tilde{z},t) = 2\pi u$ into Eqs. (10) and (11), the time-averaged intensity of the wave-packet state $I^{(\pm)} = |\Psi^{(\pm)}(x,y,z,t)|^2$ in Eq. (14) can be deduced to be localized on the distribution $I_c^{(\pm)}$:

$$I_c^{(\pm)}(x,y,z) = \frac{2}{\pi w_x(z)w_y(z)} \left\{ \sum_{u=0,1,2\cdots} e^{-\{\tilde{x}-\sqrt{2}\sqrt{m_o}\cos[(\frac{\omega_{t,x}}{\omega_z})2\pi u \mp\theta_{G,x}(z)]\}^2} e^{-\{\tilde{y}-\sqrt{2}\sqrt{n_o}\cos[(\frac{\omega_{t,y}}{\omega_z})2\pi u \mp\theta_{G,y}(z)]\}^2} \right\}. \tag{15}$$

Equation (15) reveals that the spatial distribution $I_c(x,y,z)$ of the wave-packet state is formed by the assemblage of numerous backward and forward Gaussian beams. Under the degeneracy condition given by Eq. (6), the spatial distribution $I_c(x,y,z)$ can be generally found to correspond to the 3D geometric surface with the transverse topology of Lissajous curves. To be explicit, substituting $\tilde{x} = \sqrt{2}x/w_x(z)$ and $\tilde{y} = \sqrt{2}y/w_y(z)$ into Eq. (15) and using Eq. (6) for the degenerate cavity, the mathematical parametric form for the central maxima of the spatial distribution $I_c(x,y,z)$ in Eq. (15) can be expressed as

$$x(z;u) = \sqrt{m_o}w_x(z)\cos\left[\left(\frac{P}{Q} - \beta\frac{q}{p+q}\right)(2\pi u) \mp \theta_{G,x}(z)\right]$$
$$y(z;u) = \sqrt{n_o}w_y(z)\cos\left[\left(\frac{P}{Q} + \beta\frac{p}{p+q}\right)(2\pi u) \mp \theta_{G,y}(z)\right], \tag{16}$$

with $u = 0,1,2\cdots$. Equation (16) can be directly used to manifest the geometric surfaces inside the cavity. Figure 5 depicts the 3D geometric surfaces inside the cavity for various (p,q) shown in Fig. 2(b) with $n_o = 50$, $m_o = 50$, $R = 10\,\text{mm}$, $d = 0.087\,\text{mm}$, and $\beta = 2.757\times10^{-3}$.

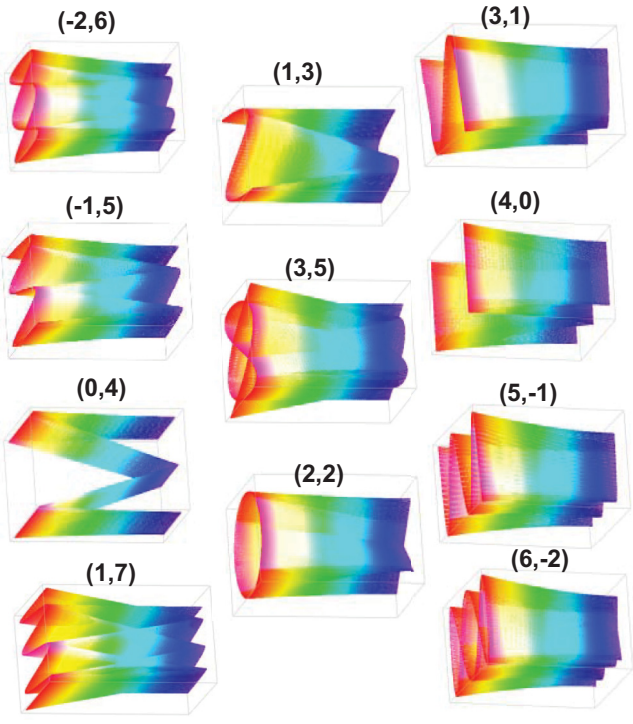

FIG. 5. Numerical results for 3D geometric surfaces inside the cavity for various (p,q) shown in Fig. 2(b) with $n_o = 50$, $m_o = 50$, $R = 10\,\text{mm}$, $d = 0.087\,\text{mm}$, and $\beta = 2.757\times10^{-3}$.

V. CONCLUSIONS

In summary, it has been theoretically verified that the symmetry breaking in spherical resonators can result in a fractal structure in the frequency spectrum as a function of the cavity length. In the fractal frequency spectrum, numerous new accidental degeneracies are found to cluster at the cavity lengths around the unperturbed degenerate cavity. Furthermore, it has been experimentally discovered that the fractal frequency spectrum can lead to the emission power varying with the cavity length in astigmatic laser resonators under the selective pumping to display a striking fractal fluctuation. We have also derived the quantum coherent states by considering the overlapping effect to manifest the noticeable finding that the wave distributions of lasing modes at the accidental degeneracies are strongly concentrated on the 3D geometric

surfaces. The present exploration can be directly applied to the 3D quantum integrable systems with symmetry breaking to derive various topological geometries of 3D coherent states.

ACKNOWLEDGMENT

This work is supported by the Ministry of Science and Technology of Taiwan (Contract No. MOST-103-2112-M-009-016-MY3).

[1] B. Mandelbrot, Science **156**, 636 (1967).
[2] B. B. Mandelbrot, *The Fractal Geometry of Nature* (Freeman, New York, 1983).
[3] M. V. Berry, J. Phys. A **29**, 6617 (1996).
[4] D. Wojcik, I. Bialynicki-Birula, and K. Zyczkowski, Phys. Rev. Lett. **85**, 5022 (2000).
[5] I. Guarneri and M. Terraneo, Phys. Rev. E **65**, 015203 (2001).
[6] H. Hegger, B. Huckestein, K. Hecker, M. Janssen, A. Freimuth, G. Reckziegel, and R. Tuzinski, Phys. Rev. Lett. **77**, 3885 (1996).
[7] A. S. Sachrajda, R. Ketzmerick, C. Gould, Y. Feng, P. J. Kelly, A. Delage, and Z. Wasilewski, Phys. Rev. Lett. **80**, 1948 (1998).
[8] T. Ogura, M. Miyamoto, A. Budiyono, and K. Nakamura, J. Phys.: Condens. Matter **19**, 092002 (2007).
[9] V. Kotimäki, E. Räsänen, H. Hennig, and E. J. Heller, Phys. Rev. E **88**, 022913 (2013).
[10] M. Brack and R. K. Bhaduri, *Semiclassical Physics* (Addison Wesley, Reading, MA, 1997).
[11] R. G. Mani and K. von Klitzing, Z. Phys. B **100**, 635 (1996).
[12] J. H. Smet, Nature **422**, 391 (2003).
[13] D. Hofstadter, Phys. Rev. B **14**, 2239 (1976).
[14] P. Streda, J. Phys. C **15**, L1299 (1982).
[15] C. Albrecht, J. H. Smet, K. von Klitzing, D. Weiss, V. Umansky, and H. Schweizer, Phys. Rev. Lett. **86**, 147 (2001).
[16] C. R. Dean, L. Wang, P. Maher, C. Forsythe, F. Ghahari, Y. Gao, J. Katoch, M. Ishigami, P. Moon, M. Koshino, T. Taniguchi, K. Watanabe, K. L. Shepard, J. Hone, and P. Kim, Nature **497**, 598 (2013).
[17] E. Schrödinger, *Collected Papers on Wave Mechanics* (AMS Chelsea Publisher, Providence, RI, 1982).
[18] P. Holland, *The Quantum Theory of Motion* (Cambridge University Press, Cambridge, 1993).
[19] R. Blüumel, *Advanced Quantum Mechanics: The Classical-Quantum Connection* (Jones and Bartlett Publishers, Sudbury MA, 2011).
[20] D. Dragoman and M. Dragoman, *Quantum-Classical Analogies* (Springer, Berlin, Heidelberg, 2004).
[21] Y. F. Chen, T. M. Huang, C. F. Kao, C. L. Wang, and S. C.Wang, IEEE J. Quantum Electron. **33**, 1025 (1997).
[22] H. Laabs and B. Ozygus, Opt. Laser Technol. **28**, 213 (1996).
[23] Y. F. Chen and Y. P. Lan, Phys. Rev. A **63**, 063807 (2001).
[24] Y. F. Chen and Y. P. Lan, Phys. Rev. A **66**, 053812 (2002).
[25] Y. F. Chen, Y. P. Lan, and K. F. Huang, Phys. Rev. A **68**, 043803 (2003).
[26] K. F. Huang, Y. F. Chen, H. C. Lai, and Y. P. Lan, Phys. Rev. Lett. **89**, 224102 (2002).
[27] T. Gensty, K. Becker, I. Fischer, W. Elsäßer, C. Degen, P. Debernardi, and G. P. Bava, Phys. Rev. Lett. **94**, 233901 (2005).
[28] J. Wiersig, Phys. Rev. Lett. **97**, 253901 (2006).
[29] Q. Song, L. Liu, S. Xiao, X. Zhou, W. Wang, and L. Xu, Phys. Rev. Lett. **96**, 033902 (2006).
[30] H. Cao and J. Wiersig, Rev. Mod. Phys. **87**, 61 (2015).
[31] J. Reithmaier, G. Sek, A. Löffler, C. Hofmann, S. Kuhn, S. Reitzenstein, L. Keldysh, V. Kulakovskii, T. Reinecke, and A. Forchel, Nature (London) **432**, 197 (2004).
[32] C. Gmachl, F. Capasso, E. E. Narimanov, J. U. Nöckel, A. D. Stone, J. Faist, D. L. Sivco, and A. Y. Cho, Science **280**, 1556 (1998).
[33] Y. F. Chen, T. H. Lu, K. W. Su, and K. F. Huang, Phys. Rev. Lett. **96**, 213902 (2006).
[34] Y. F. Chen, J. C. Tung, P. Y. Chiang, H. C. Liang, and K. F. Huang, Phys. Rev. A **88**, 013827 (2013).
[35] J. B. McManus, P. L. Kebabian, and M. S. Zahniser, Appl. Opt. **34**, 3336 (1995).
[36] J. Courtois, A. Mohamed, and D. Romanini, Phys. Rev. A **88**, 043844 (2013).
[37] D. Romanini, Appl. Phys. B **115**, 517 (2014).
[38] K. Staliunas and V. J. Sanchez-Morcillo, *Transverse Patterns in Nonlinear Optical Resonators*, Springer Tracts in Modern Physics Vol. 183 (Springer-Verlag, Berlin, 2003).
[39] M. Brambilla, F. Battipede, L. A. Lugiato, V. Penna, F. Prati, C. Tamm, and C. O. Weiss, Phys. Rev. A **43**, 5090 (1991).
[40] E. Louvergneaux, D. Hennequin, D. Dangoisse, and P. Glorieux, Phys. Rev. A **53**, 4435 (1996).
[41] V. B. Taranenko, K. Staliunas, and C. O. Weiss, Phys. Rev. Lett. **81**, 2236 (1998).
[42] P. Michler, A. Imamoğlu, M. D. Mason, P. J. Carson, G. F. Strouse, and S. K. Buratto, Nature (London) **406**, 968 (2000).
[43] J. Wiersig, C. Gies, F. Jahnke, M. Aßmann, T. Berstermann, M. Bayer, C. Kistner, S. Reitzenstein, C. Schneider, S. Höfling *et al.*, Nature **460**, 245 (2009).
[44] Q. Song, W. Fang, B. Liu, S. T. Ho, G. S. Solomon, and H. Cao, Phys. Rev. A **80**, 041807(R) (2009).
[45] G. P. Karman and J. P. Woerdman, Opt. Lett. **23**, 1909 (1998).
[46] M. A. Yates and G. H. C. New, Opt. Commun. **208**, 377 (2002).
[47] G. P. Karman, G. S. McDonald, G. H. C. New, and J. P. Woerdman, Nature **402**, 138 (1999).
[48] K. Falconer, *Fractal Geometry: Mathematical Foundations and Applications* (John Wiley & Sons, Inc., Chichester, UK, 2003).
[49] Y. F. Chen, Y. J. Huang, P. Y. Chiang, Y. C. Lin, and H. C. Liang, Appl. Phys. B **103**, 841 (2011).
[50] Y. F. Chen, Phys. Rev. A **83**, 032124 (2011).